Folke, Frederik; Wurms, Sven

Numerical estimation of bedform roughness

Numerical estimation of bedform roughness

Frederik Folke and Sven Wurms
Department of Hydraulic Engineering
Federal Waterways Engineering and Research Institute
76187 Karlsruhe, Germany
frederik.folke@baw.de

***Abstract*— An appropriate a priori estimation of the bed roughness for numerical river models is still challenging. For gravel river beds various approaches exist based on the grain-size distribution curve. But there is still a lack to estimate the roughness effect of geometrical bed structures such as rock peaks which are not resolved by the numerical grid, so-called sub-grid structures. The aim of the ongoing investigation is to provide a general method to capture sub-grid structures for individual numerical models using both TELEMAC-3D and TELEMAC-2D.**

A numerical test-bench to evaluate the roughness effect of geometrical bedform structures is introduced. For the calibration and validation a three-dimensional hydrodynamic-numerical (3D-HN) model is set up. All structures of the underlying geometry are resolved properly. For the investigation both a digital elevation model of natural rock peak structures of a shallow river bed and an artificial elevation model are used.

The coarse grid two-dimensional hydrodynamic-numerical (2D-HN) model is calibrated via the high-resolved 3D-HN model. Furthermore a statistical roughness approach for steep streams is applied to model shallow open-channel flow. The suitability of this method to capture the roughness effect of sub-grid structures is tested. Subsequently the flow over different elevated rock peaks is investigated. Beside the global water level local effects are compared and discussed.

I. INTRODUCTION

The hydraulic resistance of river flow is affected by various factors. Beside bed roughness [2] identified vegetation, channel irregularity, channel alignment, silting and scouring, obstruction, size and shape of channel, stage and discharge, seasonal change, suspended material and bedload as the factors with the greatest impact. These mechanisms do not act isolated but interact resulting in a complex physical behaviour. In all engineering applications of open-channel flow the estimation of the bed roughness is of prime importance; as it can be seen as the major calibration factor for all hydrodynamic-numerical models.

The bed roughness is influenced both by the grain size of the occurring sediments and by the geometrical structure of the bed surface. According to [3] the total hydraulic resistance of bed roughness, τ, can be interpreted as a sum of the drag force of the grain roughness, τ', and the drag force of the form roughness, τ'',

$$\tau = \tau' + \tau''. \quad (1)$$

An appropriate a priori estimation of the bed roughness for numerical river models is still challenging. For the grain roughness various approaches exist based on the grain-size distribution curve assuming a linear behaviour between a representative grain diameter and the roughness coefficient (here: equivalent sand roughness of Nikuradse, k_s) as shown in Tab. 1.

TABLE 1. GRAIN ROUGHNESS APPROACHES

Author (year)	Approach
Garbrecht (1961)	$k_s = d_{90}$
Engelund & Hansen (1966)	$k_s = 2 \cdot d_{65}$
Hey (1979)	$k_s = 3.5 \cdot d_{84}$
Kamphius (1974)	$k_s = 2 \cdot d_{50}$
Van Rijn (1984)	$k_s = 3 \cdot d_{90}$
Mertens (1997)	$k_s = 2.5 \cdot d_{50}$
Dittrich (1998)	$k_s = 2.5 \cdot d_m$ (gravel)
	$k_s = 3.5 \cdot d_{84}$ (coarse gravel)

In mobile sand and gravel bedded rivers the roughness can be significantly affected by pattern formation. For example ripples and dunes can occur in sand and sand dominated river beds acting as a roughness on the flow. To account for these geometrical shapes three different bed roughness predictors are implemented in SISYPHE to account for flat beds, rippled beds or dunes and mega ripples [6].

But there is still a lack of knowledge to estimate the roughness effect of geometrical bed structures such as rock peaks which are not resolved by the numerical grid. To investigate the effect of a modification of such sub-grid structures on the flow field an appropriate model is necessary. Up to now most researchers dealing with this subject concentrated on steep streams. Beside various approaches of other authors [5] and [1] introduced the standard deviation of the bottom elevation, s, to capture the roughness effect in steep streams

$$s = \sqrt{\frac{1}{n-1}\sum_{i=1}^{n}(z_i - \bar{z})^2}\,. \quad (2)$$

In this paper we focus on the estimation of bed roughness in large slightly sloped rivers due to geometrical structures. A numerical test-bench to evaluate the roughness effect of sub-grid structures is introduced. The aim of the ongoing investigation is gaining a deeper insight into the roughness effect of geometrical bedform structures and to provide a general method for the determination of the calibration parameter for individual numerical models using both TELEMAC-3D and TELEMAC-2D. As a first step the roughness approach of [5] and [1] for steep streams is applied to model shallow open-channel flow. Furthermore the suitability of this method is tested.

For the calibration and validation of the coarser models a high-resolution three-dimensional hydrodynamic-numerical (3D-HN) model is set up. All structures of the underlying geometry are resolved properly. The standard k-epsilon model is used to capture the turbulent structures. For the vertical velocity components the non-hydrostatic approach is used. The effect of roughness is taken into account by the implemented approach of Nikuradse. All models are operated with stationary boundary conditions. For the investigation both an artificial elevation model and a digital elevation model of natural rock peak structures of a shallow river bed are used.

After calibrating the smooth bottom case subsequently the flow over different elevated rock peaks using the above mentioned roughness model (cf. equation 1) for the sub-grid structures is investigated. Beside the global water level local effects are compared and discussed.

II. Bottom friction

A. *Definition of bottom friction in 2D and 3D*

The bottom shear stress in both horizontal directions (parallel to the bottom) is described for depth-averaged flow as (cf. [4])

$$\vec{\tau} = -\frac{1}{2} \cdot \rho \cdot C_f \cdot \vec{u} \cdot \sqrt{u^2 + v^2} \tag{3}$$

with the fluid density, ρ, the dimensionless friction coefficient, C_f, and the horizontal depth-averaged flow velocities, u and v. According to the depth-averaged formulation the bottom shear stress in 3D is described as

$$\vec{\tau} = -\frac{1}{2} \cdot \rho \cdot C_f \cdot \vec{U} \cdot \sqrt{U^2 + V^2} = \mu \frac{\partial \vec{U}}{\partial n} \tag{4}$$

with the horizontal flow velocities, U and V, the dynamic viscosity, μ, and the bottom normal vector, n.

Both in TELEMAC-2D and TELEMAC-3D various laws of bottom friction are implemented to account for the shear force at the bottom. In this paper only the formulation of Nikuradse is considered.

B. *Nikuradse law in TELEMAC-2D and TELEMAC-3D*

The friction law of Nikuradse is based on the equivalent sand roughness, k_s. Assuming a logarithmic velocity profile over the whole depth in TELEMAC-2D the bottom friction is determined by Nikuradse law as

$$\vec{\tau} = -\rho \cdot \left(\frac{\kappa}{\ln\left(\frac{H \cdot 11.036}{k_s}\right)} \right)^2 \cdot \vec{u} \cdot \sqrt{u^2 + v^2} \tag{5}$$

with the water depth, H, and the von Kármán constant, κ. In TELEMAC-3D the logarithmic velocity profile is constrained only for the bottommost layer resulting in the following assumption for the bottom shear stress

$$\vec{\tau} = -\rho \left(\frac{\kappa}{\ln\left(\frac{30 \cdot \Delta z}{k_s}\right)} \right)^2 \cdot \left(U^2 + V^2\right) \tag{6}$$

with the height of the first layer, Δz. The velocity profile in the layers above is part of the 3D solution.

III. Numerical Model

To investigate the effect of geometrical bedforms a numerical test-bench is introduced. In a slightly sloped rectangular channel different bedform structures are inserted in a defined test section. The elevation of the structures will be modified by a scaling factor to evaluate their impact on the flow field. In the reference model all geometrical structures are resolved using TELEMAC-3D with the non-hydrostatic approach and the standard k-epsilon turbulence model. For a proper representation of the turbulent flow structures the widely-used two-equation k-epsilon model is used instead of an algebraic model or defining a constant viscosity.

Different cases both in TELEMAC-2D and TELEMAC-3D with representative mesh size values for numerical models of German waterways, such as River Rhine, Danube etc. at BAW are setup. The bottom elevation is defined by a mesh dependent patch averaging.

In a first step the smooth channel case will be calibrated for the particular variants. Subsequent different bedforms are investigated using the reference setup. The influence on the water level differences of the geometrical structures are compared and discussed. Finally the statistical approach of [5] and [1] is applied to the present cases with different geometrical structures. Both with TELEMAC-2D and TELEMAC-3D the method is evaluated according to capture the non-resolved geometrical structures.

A. *Geometry and boundary conditions*

The channel has a horizontal size of 2000 m x 50 m and a slope of 0.63‰ (illustrated in Fig. 1). The sidewalls are modelled with the slip-boundary condition. The section with the geometrical roughness elements starts and ends with a

distance 500 m of each inlet and outlet to minimize the effect of the upstream and downstream boundary conditions.

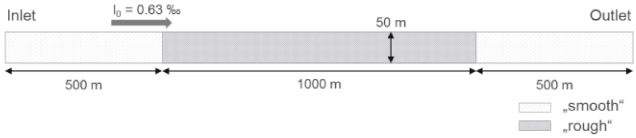

Figure 1. *Test channel geometry (topview)*

Three different discharge events are investigated according to low water level, mean water level and a high-water level of the Middle Rhine (cf. Tab. 2). The relevant flow is analytically determined using the empirical Darcy-Weisbach equation.

TABLE 2. BOUNDARY CONDITIONS

Event	Water depth	Flow
Low water	H = 3 m	Q = 320 m³/s
Mean water	H = 5 m	Q = 750 m³/s
High water	H = 7 m	Q = 1295 m³/s

B. *Bottom elevation / geometrical structures*

Beside a complete smooth channel two different geometrical structures as shown in Fig. 2 are investigated. The rock peak structures are extracted from the riverbed of the Middle Rhine in the slate mountains with a maximum elevation of -0.84 m and +0.68 m and with a standard deviation of 0.23 m. The “artificial” structures are generated by a superposition of two sinusoidal waves

$$z = A \cdot \left(\sin\left(\frac{x \cdot 2\pi}{\lambda}\right) \cdot \cos\left(\frac{y \cdot 2\pi}{\lambda}\right) \right) \quad (7)$$

with the amplitude, A, and the wavelength, λ.

The mean bottom level of all cases is the same. The inlet and outlet sections are smooth (Fig. 1). The overall grain roughness in the reference case is 0.075 m.

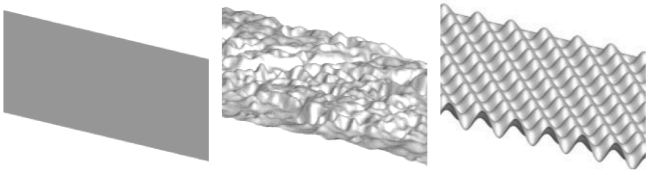

Figure 2. *Bottom elevation, 5x superelevated (left: smooth, center: rock peaks, right: artificial)*

To investigate the influence of the height and the slope of the peaks the structures are both scaled (a) only vertically (z-direction) and (b) in all directions (uniform) as sketched in Fig. 3.

In Tab. 3 all geometrical variants of the presented study are listed leading to a total number of 12 channel bed structures – the smooth case, 4 rock peaks variants and 7 variants with an artificial geometrical structure.

Figure 3. *2D-sketch of rock peaks (left: original, center: scaled in vertical direction (a), right: scaled in vertical and horizontal direction (b))*

In Tab. 3 all geometrical variants of the presented study are listed leading to a total number of 12 channel bed structures – the smooth case, 4 rock peaks variants and 7 variants with an artificial geometrical structure.

TABLE 3. OVERVIEW OF GEOMETRICAL VARIANTS

Structure Case	Scaling factor (FS) / Wavelength (λ) and amplitude (A)
Smooth	FS = 0 / A = 0
Rock peaks	FS = 1
	FS = 0.8 (z-direction)
	FS = 0.5 (z-direction)
	FS = 0.5 (uniform)
Artificial	λ = 4, A = [0.25, 0.5]
	λ = 8, A = [0.25, 0.5]
	λ = 12, A = [0.25, 0.375, 0.75]

C. *Meshes*

In the reference case (TELEMAC-3D) the geometrical structures are resolved with an average horizontal mesh size of 0.3 m. For the vertical direction 30 sigma-layers are used resulting in a large mesh size of approximately 77 million 3D-elements.

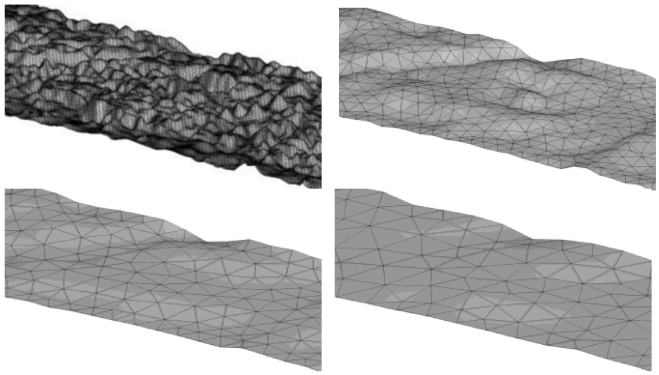

Figure 4. *Bottom elevation (rock peaks) for different mesh resolutions, 5x superelevated (topleft: reference, topright: grid 3 m, bottomleft: grid 5 m, bottomright: grid 7 m)*

For the variants an average mesh size of 3 m, 5 m and 7 m is chosen, according to mesh size values for numerical models of large rivers such as River Rhine at BAW. Geometrical information of sub-grid structures – structures smaller than the mesh size – is getting lost. This phenomenon is illustrated in Fig. 4. The bottom elevation is defined by a mesh dependent patch averaging. For the evaluation of the bottom elevation of a cell node all points of the elevation model within the adjacent elements are considered. The

method is not explained in detail here. An overview of all three meshes including the number of elements is given in Tab. 4.

The Elder turbulence model in the TELEMAC-2D cases is chosen analogously to preceding study. For "grid 5 m" at low water level no difference in the water level was observed comparing the Elder and k-epsilon turbulence model in TELEMAC-2D. These results are not shown in here. Further investigations of the influence of the turbulence modelling approaches are not part of the present study.

TABLE 4. OVERVIEW OF MODELS AND MESH SIZES

	Dim.	Turb. model	2D-Elements	Sigma-Layers	3D-Elements
Reference	3D	k-epsilon	2'560'704	30	76'821'120
Grid 3 m	2D	Elder	19'496	-	-
Grid 5 m			6'454	-	-
Grid 7 m			3'590	-	-
Grid 3 m	3D	k-epsilon	19'496	10	194'960
Grid 5 m			6'454	10	64'540

IV. RESULTS

To compare the results the free surface is extracted along the x-axis (with x in direction from inlet to outlet) in the middle of the channel. For a quantitative comparison the water level difference, ΔH_{1200m}, 100 m before and after the rough section is evaluated

$$\Delta H_{1200m} = H_{x=400m} - H_{x=1600m}. \quad (8)$$

The location with a certain distance to the rough section is chosen to avoid local roughness effects without averaging the results over the channel width.

A. Calibration (smooth bed)

In a first step the TELEMAC-2D and TELEMAC-3D with an average mesh size of 3 m, 5 m and 7 m (latest only TELEMAC-2D) are calibrated via the highly resolved TELEMAC-3D reference results.

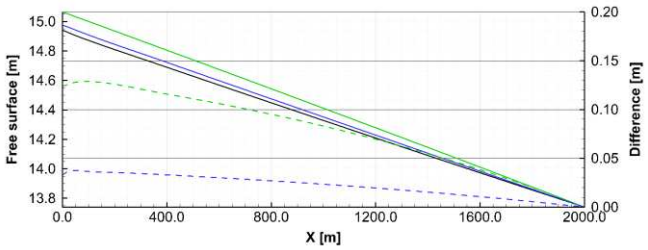

Figure 5. *Free surface along mean flow direction at mean water level with a grain roughness of 0.075 m (solid lines; black: reference, green: grid 3m 2D, blue: grid 3m 3D) and water level difference to reference case (dashed lines)*

In Fig. 5 the free surface at mean water and the water level differences of the reference case and of the variants with an average mesh size of 3 m, both TELEMAC-2D and TELEMAC-3D are shown with a grain roughness of 0.075 m. The TELEMAC-2D case shows the highest free surface elevations which can be concluded in the highest energy losses along the x-axis. For a fitting of cases a reduction of the grain roughness is necessary. The results for the calibration of all cases are summarized in Tab. 5.

The TELEMAC-2D cases can be fitted to the reference results with a grain roughness of 0.047 m and the TELEMAC-3D cases with a grain roughness of 0.065 m for all three discharge events. The influence of the average mesh size between 3 m and 7 m is negligible both for the TELEMAC-2D and the TELEMAC-3D cases (cf. Tab. 5).

TABLE 5. RESULTS OF GRAIN ROUGHNESS CALIBRATION (SMOOTH BED)

	Dim.	Grain roughness	Deviation $(\Delta H_{1200m}-\Delta H_{1200m,ref})/\Delta H_{1200m,ref}$		
			Low	Mean	High
Reference	3D	k_s = 0.075 m	-	-	-
Grid 3 m	2D	k_s = 0.075 m	+8 %	+11 %	+12 %
		k_s = 0.047 m	±0 %	±0 %	+1 %
Grid 5 m		k_s = 0.075 m	+8 %	+11 %	+12 %
		k_s = 0.047 m	±0 %	±0 %	±0 %
Grid 7 m		k_s = 0.075 m	+8 %	+11 %	+12 %
		k_s = 0.047 m	±0 %	±0 %	±0 %
Grid 3 m	3D	k_s = 0.075 m	+2 %	+3 %	+3 %
		k_s = 0.065 m	±0 %	±0 %	±0 %
Grid 5 m		k_s = 0.075 m	+2 %	+3 %	+3 %
		k_s = 0.065 m	±0 %	±0 %	±0 %

The considerable difference between the highly resolved TELEMAC-3D reference case and the TELEMAC-2D case is beside numerical impacts such as numerical diffusion mostly due to the different vertical velocity profiles. The assumption of a logarithmic profile in TELEMAC-2D cannot be verified within the TELEMAC-3D reference case. Fig. 6 shows the vertical velocity profiles of the TELEMAC-3D reference case (k_s=0.075 m) and the TELEMAC-2D case with an average mesh size of 5 m (k_s=0.075 m and k_s=0.047 m) at mean water level extracted at approximately x=1200 m. The logarithmic velocity profiles for the TELEMAC-2D cases are determined based on the friction velocity, U^*, and the grain roughness, k_s (cf. [4])

$$\frac{U}{U^*} = \frac{1}{\kappa} \cdot \ln\left(\frac{y}{k_s}\right) + 8.5 \quad . \quad (9)$$

The assumption of hydraulically rough flow is in all cases valid.

With the reduced grain roughness the water level and thus the depth-averaged velocity of the TELEMAC-2D cases can be calibrated via the reference results but with different values for the bottom shear stress and the maximum values of the velocity at the free surface. This is due to the non-matching vertical velocity profiles.

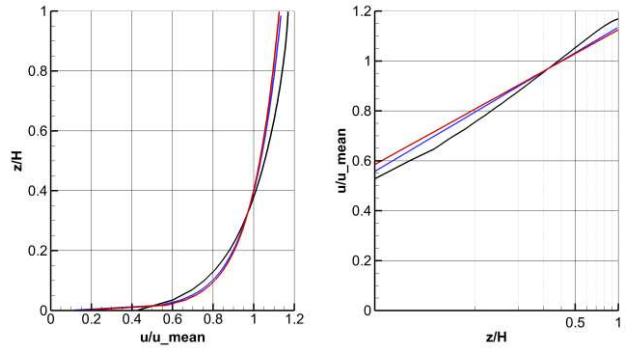

Figure 6. *Vertical velocity profiles at mean water level (black: reference, , k_s=0.075 m; blue: TELEMAC-2D, grid 5 m, k_s=0.075 m; red: TELEMAC-2D, grid 5 m, k_s=0.047 m)*

B. Resolved bedform roughness (reference model)

The influence of the geometrical bedform structures is both investigated for the rock peaks and for the artificial structures using the highly resolved reference setup.

The shape of the channel bottom has a significant impact on the velocity field which can be observed by both geometrical structures. In Fig. 7 and Fig. 8 the depth-averaged scalar velocity distribution at mean water level is shown for the rock peak structures and the artificial geometry, respectively. The scaling is chosen analogue to the mean depth-averaged velocity in the smooth case. In both cases the shape of the bottom geometry can be found also in the velocity field. With higher bottom elevations this influence is getting more significant.

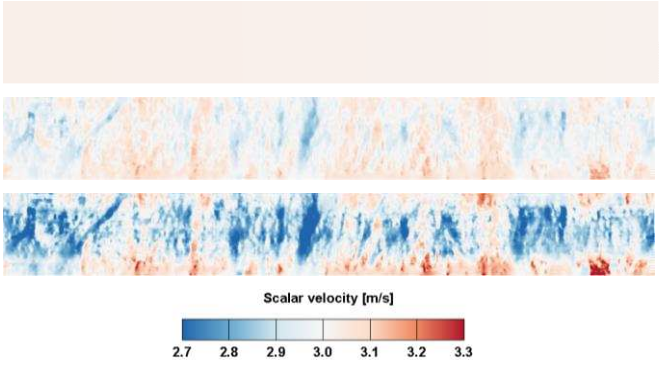

Figure 7. *Depth-averaged scalar velocity at mean water level of reference cases "rock peak structures", section x = 800 m to x = 1200 m (top: FS = 0 (smooth), center: FS = 0.5, bottom: FS = 1.0)*

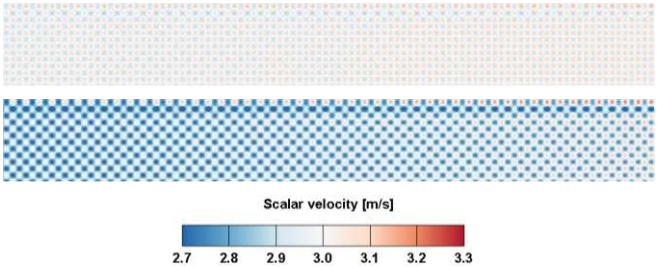

Figure 8. *Depth-averaged scalar velocity at mean water level of reference cases "artificial structures" with λ=12 m, section x = 800 m to x = 1200 m (top: A = 0.25 m, bottom: A = 0.5 m)*

In Fig. 9 the resulting water level difference, ΔH_{1200m} , for the rock peaks structures is plotted against the vertical scaling factor. The scaling factor FS=0 describes the smooth bed case. With an increasing scaling factor the water level difference, ΔH_{1200m} , is getting larger. This can be explained by the corresponding behaviour of the ratio, e,

$$e = \frac{\Delta z}{H} \tag{10}$$

with the elevation of the bedform structures, Δz, and the water depth, H. For constant discharge conditions the ratio, e, is increasing with an increasing scaling factor.

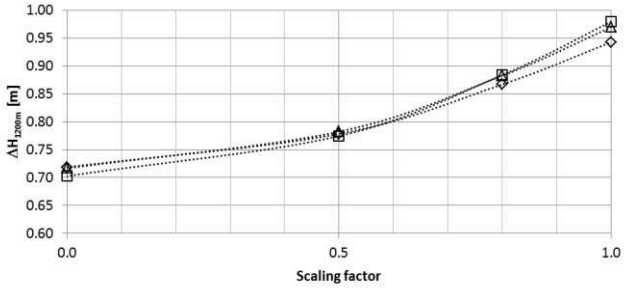

Figure 9. *Water level differences, ΔH_{1200m}, of the resolved "rock peak structures" with different geometrical scaling factors in vertical direction (◇ low water, △ mean water, □ high water)*

Differences associated with different discharge conditions are relatively small. The maximum deviation occurs for the original rock peaks structures without scaling.

The results show a non-linear behaviour between the water level difference, ΔH, and the elevation of the rock peaks structures for all water levels– especially for scaling factors greater than 0.5.

Due to the vertical scaling of the bedform structures the local gradient in the horizontal directions of the rock peaks is changing (cf. Fig. 3). The influence of the scaling only in vertical direction compared to a uniform scaling in all directions – without changing of the gradients – is shown in Fig. 10 for a scaling factor of 0.5. For all water levels the change is relatively small.

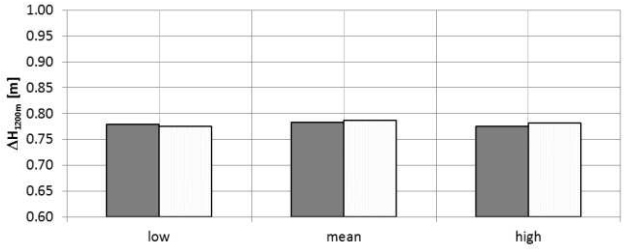

Figure 10. *Water level differences, ΔH_{1200m}, of reference cases "rock peak structures" with geometrical scaling factors of 0.5 (filled: scaled in vertical direction, hollow: scaled in all directions)*

The non-linear behaviour between the differences of the water level, ΔH_{1200m}, and the bedform elevation is also observed for the artificial structures as shown in Fig. 11.

For the artificial structures, composed of sinusoidal waves, the scaling only in vertical direction compared to a uniform scaling has an impact. The variants "λ=4 m, A=0.25 m", "λ=8 m, A=0.50 m" and "λ=12 m, A=0.75 m" result all in a similar water level difference (cf. Fig. 11). All three cases have the same gradients in horizontal directions but different elevations. This phenomena can also be observed comparing the variants "λ=8 m, A=0.25 m" and "λ=12 m, A=0.375 m".

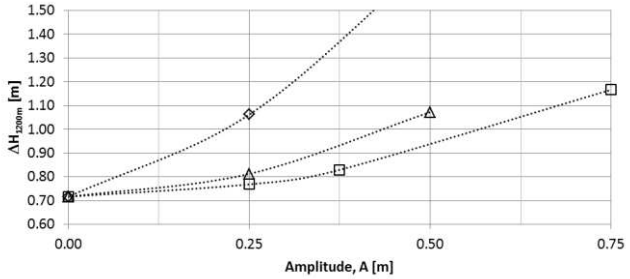

Figure 11. *Water level differences, ΔH_{1200m}, of reference cases "artificial structures" at mean water level with different amplitudes (◇ λ=4 m, △ λ=8 m, □ λ=12 m)*

Contrary to the rock peaks the bedform structure of the artificial elevation model is homogeneous and steady over the whole region. This might lead to different behaviour of the influence of the local gradients and the total elevation.

Similar to the results of the rock peaks structures the influence of the discharge on the water level differences is small for the artificial bedform structures as shown in Fig. 12 for a wavelength, λ, of 12 m.

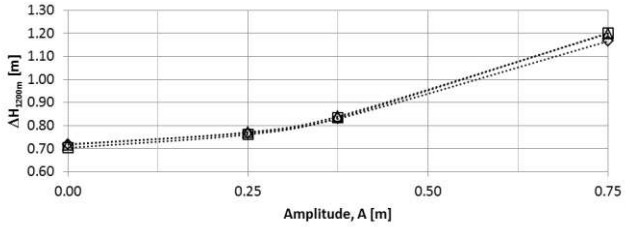

Figure 12. *Water level differences, ΔH_{1200m}, of reference cases "artificial structures" with λ=12 m and different amplitudes (◇ low water, △ mean water, □ high water)*

C. *Statistical roughness approach*

For the coarser meshes with an average size of 3 m, 5 m and 7 m effects of non-resolved geometrical structures have to be represented via the roughness model. Based on the approach of [5] and [1] the total Nikuradse roughness, $k_{s,sum}$, is determined as the sum of the calibration grain roughness, $k_{s,cal}$, and the grid dependent standard deviation of the bottom elevation, s, multiplied by a weighting factor, w,

$$k_{s,sum} = k_{s,cal} + w \cdot s. \qquad (11)$$

Fig. 13 shows the resulting water level differences, ΔH_{1200m}, for both the TELEMAC-2D and TELEMAC-3D cases compared to the reference case at mean water. The applied approach of the standard deviation of the bottom elevation shows a linear behaviour between the water level difference and the bottom elevation. With increasing weighting factor the slope is getting steeper.

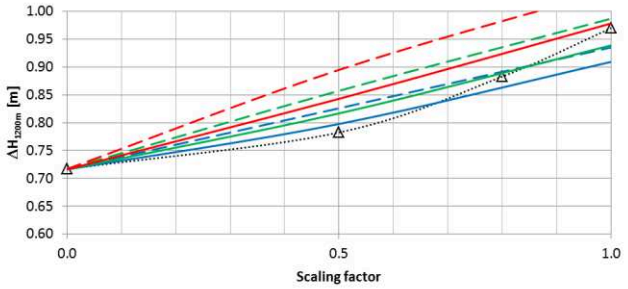

Figure 13. *Water level differences, ΔH_{1200m}, for case "rock peak structures" at mean water with different geometrical scaling factors in vertical direction (△ reference case, solid lines: TELEMAC-2D, dashed lines: TELEMAC-3D) and different weightening factors of the standard deviation of the bottom (red: s·0.5, green: s·0.7, blue: s·1.0)*

Due to its linear behaviour the approach of [5] and [1] cannot capture the roughness effect of the non-resolved geometrical rock peaks with a single weighting factor for the different scaling factors of the geometrical bedform structures.

V. Summary and Conclusion

To gain deeper insight into the roughness effect of geometrical bedform structures a numerical test-bench is successfully introduced. With a highly resolved mesh in both horizontal and vertical direction using TELEMAC-3D with the standard k-epsilon turbulence model and the non-hydrostatic approach different geometrical structures are investigated. Two different elevation models are investigated – natural rock peaks and an artificial structure composed of sinusoidal waves.

For the smooth highly resolved TELEMAC-3D reference case a non-logarithmic velocity profile was observed. The coarser resolved TELEMAC-2D and TELEMAC-3D cases could be calibrated both with a single grain roughness for all three water levels.

Vertical scaling of geometrical structures with a constant mean bottom elevation shows both for the rock peaks and for the artificial bedform structures a non-linear dependency between the bottom elevation and the differences in the water level. The influence of a uniform scaling of the geometrical structures on the water level differences appears different in the two cases.

The non-linear behaviour of geometrical roughness versus the water level difference could not be modelled using the roughness approach based on the standard deviation of the bottom elevation with a single weighting factor for the different scaling factors. Further investigation is necessary to provide a general method for the modelling of sub-grid structures. An obvious approach would be to introduce a

weighting exponent for the standard deviation of the bottom elevation. But this would lead to non-conformity in units between form and grain roughness values.

For numerical investigations in river engineering it is of great importance to capture the occurring roughness effects. The current study illustrates the complexity of geometrical bedform structures and their modelling. For an appropriate a priori estimation of these effects further research is necessary.

There is a need to bear in mind that the capability of TELEMAC-3D for such highly resolved meshes is to the authors' knowledge up to now not tested and validated in detail. Furthermore, the influence of numerical effects like numerical diffusion and the influence of the turbulence models were not evaluated in the present study.

ACKNOWLEDGEMENT

The authors thank Rebekka Kopmann for the fruitful discussions and reading the manuscript.

REFERENCES

[1] J. Aberle, "Untersuchung der Rauheitsstruktur zur Bestimmung des Fließwiderstandes in Gebirgsbächen unter Klarwasserabfluss", Mitt. des Instituts für Wasserwirtschaft und Kulturtechnik, Univ. Karlsruhe, Heft 207, 2000

[2] V.T. Chow, "Open-channel hydraulics", McGraw Hill International Book Company. Tokyo, Japan, 1983

[3] H.A. Einstein, and N. Barbarossa, "River channel roughness." Transactions ASCE, 1952, Vol. 117, Paper no. 2528, pp.1121-1146

[4] J.-M. Hervouet, "Hydrodynamics of free surface flows: modelling with the finite element method", Wiley, Chichester 2007

[5] M. Rosport, "Fließwiderstand und Sohlstabilität steiler Fließgewässer unter Berücksichtigung gebirgsbachtypischer Sohlstrukturen", Mitt. des Instituts für Wasserwirtschaft und Kulturtechnik, Univ. Karlsruhe, Heft 196, 1998

[6] P. Tassi and C. Villaret, "Sisyphe v.6.3 User's Manual", EDF R&D, 2014